Journal of Solid State Electrochemistry (2019) 23:1829–1836
https://doi.org/10.1007/s10008-019-04285-7

ORIGINAL PAPER

Evaporation induced uniform polypyrrole coating on CuO arrays for free-standing high lithium storage anode

Yulin Zhou[1] · Xiujuan Jin[1] · Jing Ni[1] · Shaofeng Zhang[1] · Jiao Yang[1] · Pengfei Liu[1] · Zhaowu Wang[1,2] · Jianfei Lei[1,3]

Received: 21 February 2019 / Revised: 18 April 2019 / Accepted: 25 April 2019 / Published online: 11 May 2019

Abstract

Polypyrrole (PPy) used as popular coatings can improve the electrochemical performance of electrodes greatly; however, uniform coatings of PPy on nanostructures is a challenging task in a solution system. Substitution for liquid phase polymerization reaction, herein a developed evaporation method is reported to make pyrrole vapor in situ polymerization on CuO arrays for the uniform PPy coatings. With the help of this uniform PPy coatings, the unique structure of arrayed CuO film can well maintain the stability of mechanical structures and has rapid transmission of lithium ions and electrons during charge/discharge processes, hence harvesting a high lithium storage. Electrochemical tests indicate that PPy can not only enhance the specific capacities of CuO anodes greatly but also improve the cyclic stability at a high-current density. The specific capacity of the CuO@PPy integrated anode can be up to 561 mAh g^{-1} at 1 C after 100 cycles, which is increased by almost 33% than that of the pure CuO anode.

Keywords Electrochemistry · Lithium ion battery · Conductive polymer · Free-standing · Cupric oxide

Introduction

Due to the higher specific capacity than graphite, transition metal oxides (TMO, 600–800 mAh g^{-1}) have attracted much attention recently and have been considered as one of the most promising anode materials for the next generation lithium ion batteries (LIB) [1–7]. Cupric oxide (CuO) is an important TMO, and it has been widely studied in photocatalysis [8, 9] and LIB [10–13]. When used as anode material, CuO usually displays large resistance and poor rate performance due to its poor electron and lithium conductivity. Moreover, the remarkable volume variation during the lithium intercalation/extraction leads to rapid capacity decay [14, 15]. Many strategies have been proposed to address these challenges and improve lithium storage performance, including preparing coated nanostructures [16–18], fabricating 3D hierarchical structures [19], introducing foam collectors [20–23], and designing free-standing electrode systems [24, 25]. Although these efforts have achieved tremendous success, CuO anodes exhibit a high irreversible capacity loss in each cycle because of the continuous formation of solid electrolyte interface (SEI) films. Moreover, once a high-current density is applied on the anodes, the electrode film will collapse instantaneously, and its capacity also drops rapidly to a low level, especially seriously in slurry electrodes. It is well known that in slurry electrodes, additional agents, such as conductors and binders, must be required to enhance contact between active materials effectively and integrate coatings with current collectors firmly. Undoubtedly, the binders not only reduce the energy density of the battery but also block the transmission of electrons and lithium, thus lowering the performances of battery. In view of these drawbacks, it is encouraged and crucial to develop free-standing electrodes for high performances of the batteries.

Free-standing electrodes are fabricated without using any polymer binders, and many researches have employed free-standing electrodes to overcome the problems mentioned above [26–30]. Some works have focused on incorporating CuO into a flexible matrix, such as carbon nanotube webs [31]

✉ Xiujuan Jin
happyjuan610@163.com

✉ Jianfei Lei
leijianfei9966@163.com

[1] School of Physics and Engineering, Henan University of Science and Technology, Luoyang 471023, China

[2] National Laboratory of Solid State Microstructures, Nanjing University, Nanjing 210093, China

[3] Henan Key Laboratory of Photoelectric Energy Stroage Materials and Applications, Henan University of Science and Technology, Luoyang 471023, China

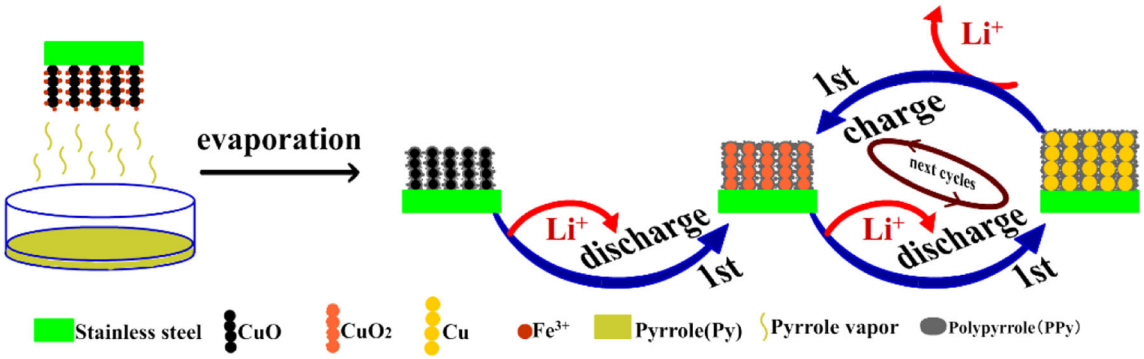

Fig. 1 Schematic diagram of preparation process and the discharge/charge cycles for CuO@PPy integrated anode

and graphene sheets [32]. Others have employed advanced technologies for in-situ growth of CuO on the metal collectors, such as magnetron sputtering [33–35] and electrochemical deposition [36]. In this work, CuO anodes are fabricated by an electrochemical deposition method to form arrayed architectures, in which ordered interspaces among arrays can accommodate volume expansion efficiently. However, it is found that the ordered structure alone is not enough to ensure a high rate performance and a high lithium storage capacity, and usually conductive coating [37, 38] or employing solid electrolyte is necessary. Polypyrrole (PPy) is a favorite conductive polymer and has been used as conductive coating layers to improve the electrochemical performance of electrodes [39–42]. In numerous reports, PPy coating layers are usually prepared by electrochemical [43] or chemical [44, 45] oxidation techniques from pyrrole monomers in a liquid phase system. The electrochemical polymerization is not suitable for scaling up and cannot be used with non-conducting surfaces, while the traditional chemical oxidation has challenge for forming uniform coating layers due to the easy agglomeration of PPy. In this regard, we develop an evaporation method to make pyrrole vapor in situ polymerization on CuO arrays for

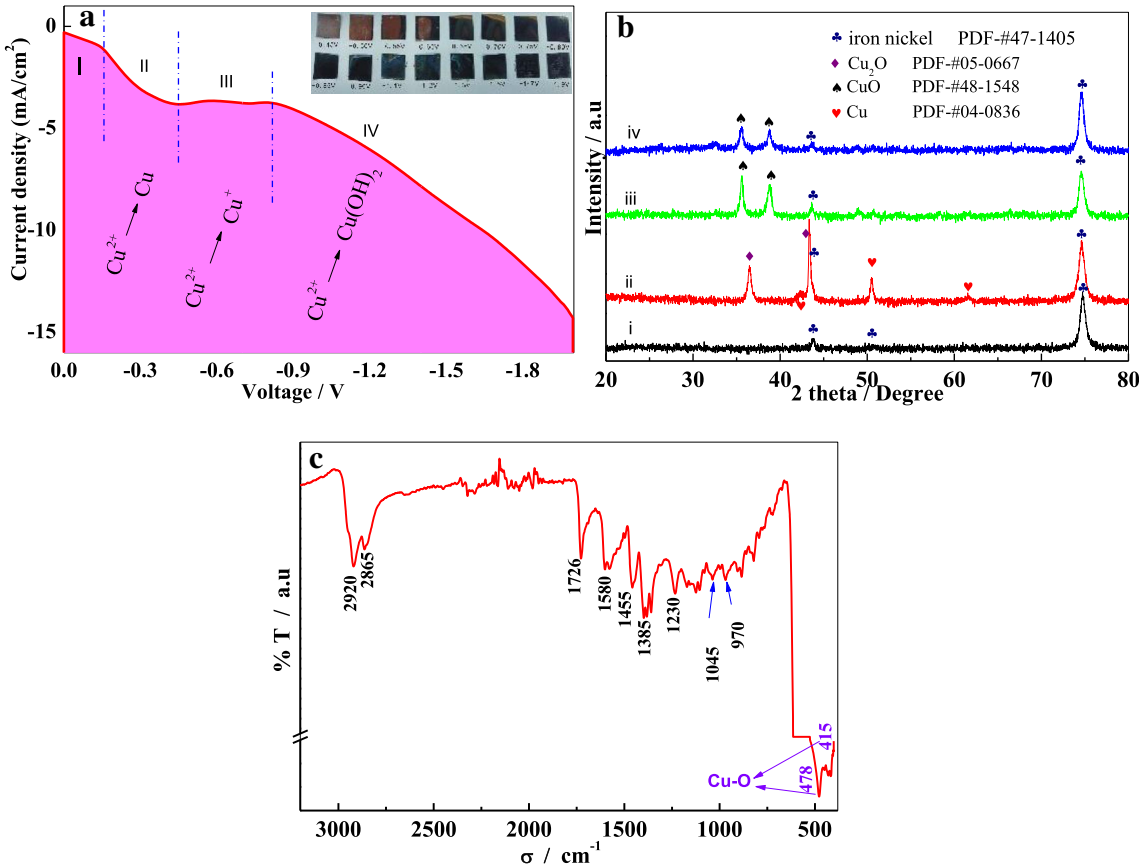

Fig. 2 **a** Potentiodynamic curve to determine the preparation potential of CuO, **b** XRD diffraction patterns of stainless steel substrate (i), initial sample before calcinations (ii), CuO sample after calcinations (iii) and CuO@PPy sample (iv) and **c** the FT-IR spectroscopy of the CuO@PPy sample

the uniform coatings (as shown in Fig. 1). It is found that, with the help of this uniform PPy coating, the prepared CuO film can well maintain the stability of mechanical structures. Also, the uniform coatings can accelerate the transmission of lithium ions and electrons during the discharge/charge processes, hence harvesting a high lithium storage and better c-rate performance.

Experimental

Materials synthesis

In this work, CuO arrays were prepared by electrochemical deposition, which was performed on an electrochemical system (chi650E, Shanghai, China) by a typical three-electrode system. The working electrode was 304 stainless steel exposed one side of 1 × 1 cm^2 conductive surface, and the counter electrode was a platinum foil with a large area. A saturated calomel electrode (SCE) was used as a reference electrode and the deposition solution was 15 mmol L^{-1} $Cu(NO_3)\cdot 3H_2O$. We carried out deposition experiments with a potentiostatic method at room temperature and negative voltage of − 0.82 V (vs. SCE) had been applied for 13 min. After deposition, the as-prepared films were removed from the bath immediately and rinsed with deionized water, and then dried in a stream of N_2 gas before being calcined in an oven at 450 °C under air atmosphere for 150 min.

PPy Coatings were prepared by an evaporation method to make pyrrole vapor in situ polymerization on CuO arrays for the uniform coatings. The coating process is as shown in Fig. 1. The as-prepared CuO film was immersed in 0.1 mol L^{-1} $FeCl_3$ solution to load Fe^{3+} ions. After being dried in the oven at 60 °C completely, the film was transferred into a sealed culture dish containing 0.5 mol L^{-1} pyrrole in ethanol solution for 24 h at room temperature. During this period, pyrrole monomers were slowly vaporized together with alcohol to form vapors, which reacted with Fe^{3+} adhering to the surface of CuO to form uniform PPy coatings. Before being dried completely, the film was washed with ultrapure water to remove the surplus Fe^{3+}.

Materials characterization

The morphologies of the samples were examined by a field-emission scanning electron microscopy (FE-SEM; ZEISS Ultra, Germany) and crystallographic information for the sample was investigated with X-ray powder diffraction (XRD; Bruker D8 Advance, Germany).

Electrochemical measurements

The electrochemical measurements were carried out by using CR 2025 coin-type cells. The working electrode was the as-prepared films. Lithium foil was used as both the counter electrode and the reference electrode. The cell was assembled

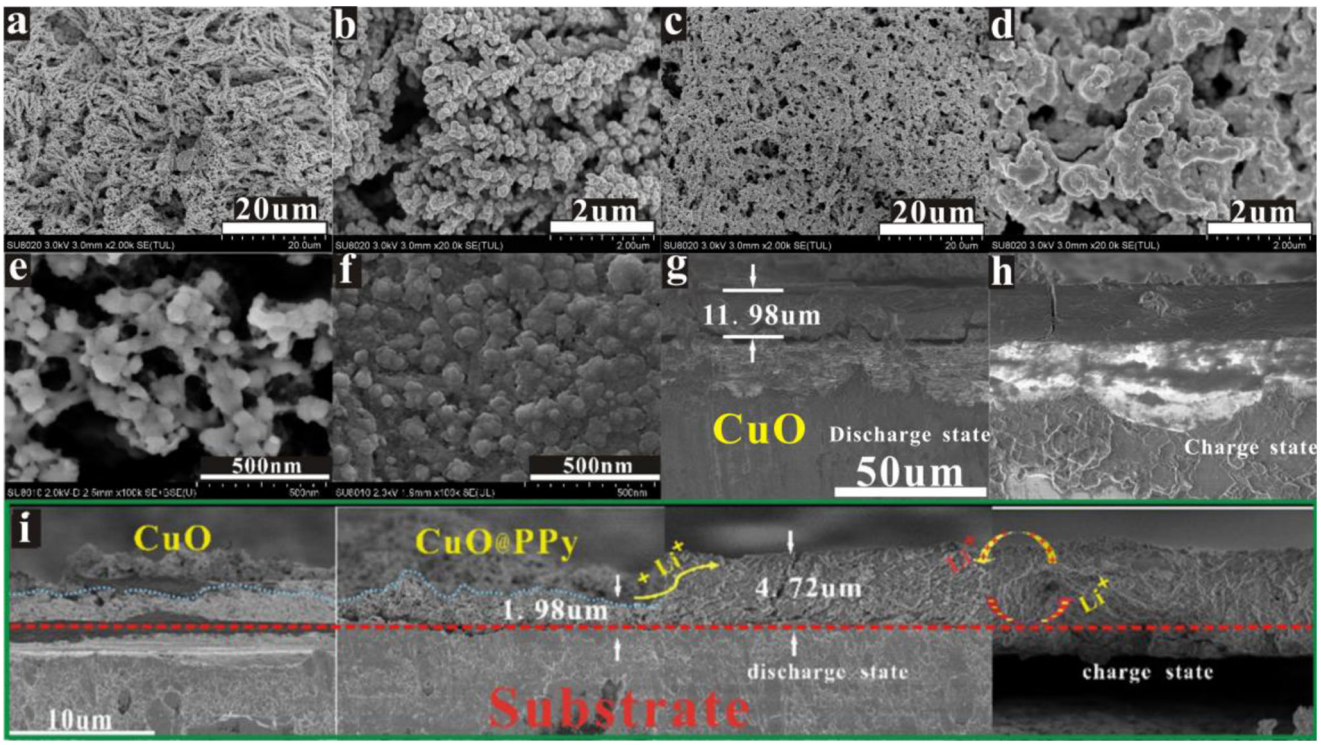

Fig. 3 **a**, **b** SEM images of pure CuO and **c**, **d** CuO@PPy anode before cycle and **e**, **f** after 100 cycles, respectively; the cross-sectional images of samples from pure CuO to **g**, **h** the 100th charge and **i** CuO@PPy

in a high purity argon-filled glove box. A microporous polypropylene membrane (Cellgard 2300) was used as the separator, and the electrolyte was $LiPF_6$ (1.0 mol L^{-1}) in a 1:1 (*w*:*w*) mixture of ethylene carbonate (EC) and dimethyl carbonate (DMC). Charge/discharge tests were performed using a LANHE battery testing system (CT2001A, Wuhan, China) at different current rate with a voltage windows of 0.05–3 V (vs. Li^+/Li).

Results and discussion

It is challenging to obtain pure CuO samples by electrochemical deposition due to the variable valence of copper. Figure 2a displays the potentiodynamic curve helping to set an appropriate potential for preparing CuO samples. It can be seen that the curve is divided into four voltage regions roughly, which corresponds to different reactions. Combining with the color changing of the samples, we can infer that Cu^{2+} ions are mainly reduced to Cu at lower deposition potentials (range II) while are combined with OH^- ($NO_3^- + H_2O + 2e^- \rightarrow NO_2^- + 2OH^-$) to form $Cu(OH)_2$ or Cu $(NO_3)_2 \cdot 3Cu(OH)_2$ at higher deposition potentials (range IV). In view of the quality of the films and the efficiency and facility of the preparation process, we select − 0.82 V within the range III as the deposition potential in this work. XRD diffraction patterns indicate that samples prepared by electrochemical deposition before calcination are composed of Cu and Cu_2O (Fig. 2b-ii) and have been changed to CuO completely after calcination at 450 °C for 150 min (Fig. 2b-iii). To further confirm the presence of PPy in CuO@PPy sample, the Fourier transform infrared (FT-IR) was carried out, and the result was shown in Fig. 2c. Clearly, the characteristic peaks at 2920 and 2865 cm^{-1} are ascribed to the stretching vibration of C-H, 1580 and

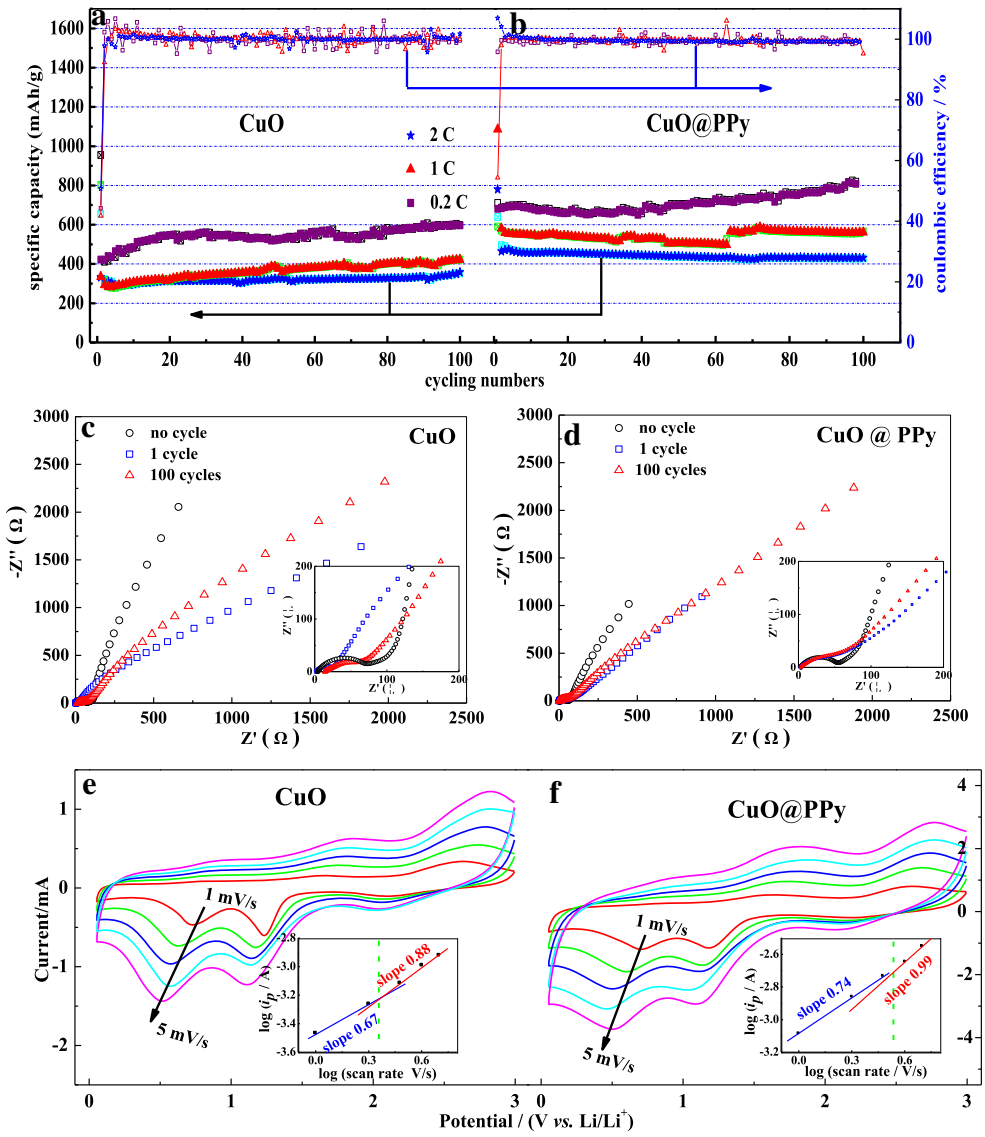

Fig. 4 The cyclic performances and coulombic efficiencies, impedance curves at different cycles, and CV curves at different scan rates from 1 to 5 mV s^{-1}, and the determination of the slope values calculated by peak current and scan rate at reduction states (insert plots); **a**, **c**, **e** pure CuO and **b**, **d**, **f** CuO@PPy

Table 1 Discharge specific capacities of the 1st and the 100th for CuO and CuO@PPy anodes at various current densities

	CuO/mAh g^{-1}			CuO@PPy/mAh g^{-1}			Improved/%	
	1st	2nd	100th	1st	2nd	100th	1st	100th
0.2 C	955	411	598	710	686	808	25 ↓	35.1 ↑
1 C	802	317	422	1086	581	561	35.4 ↑	32.9 ↑
2 C	650	322	351	781	464	432	20.2 ↑	23.1 ↑

1455 cm^{-1} are due to the antisymmetric and symmetric ring-stretching modes of the PPy rings [46], and 1385, 1280, 1045, 970 cm^{-1} are indexed to C-N stretching, C-N in-plane deformation, C=C-H the in-plane and out-of-plane deformation vibrations in the pyrrole ring, respectively [47, 48]. There are two strong absorption bands observed at about 478 and 415 cm^{-1} in the low wavenumber region assigning to the Cu-O stretching vibration [42]. The above results indicate that the CuO@PPy composite films are successfully prepared.

It can be seen from Fig. 3a that the prepared CuO film is composed of uniform particles to form ordered architectures, and the size of each particle is about 100–130 nm. More carefully, observing from Fig. 3b, we found these particles are aggregated from smaller nanoparticles (less than 15 nm). It is well known that, in order to solve the volume changing problems, one effective way is to create nanostructured CuO, and we believe the prepared CuO here can also play an important role in solving the capacity fading of CuO. Also, plenty of gaps can be found between particles, and undoubtedly these gaps can not only accommodate the volume expansion and relieve the stress caused by the expansion of CuO during the discharge processes but also provide convenience for in situ polymerization of pyrrole. Figures 3 c and d show SEM images of the coated CuO sample with PPy by the evaporation method. Clearly, no agglomeration of PPy can be observed and the coating layer is found to be uniform on CuO arrays. Due to the uniform coatings, ordered CuO@PPy nanostructures can well maintain the stability of mechanical structures during the charge/discharge processes. As shown in Fig. 3 e and f, it can be seen that the structures of the pure CuO have almost collapsed and few active materials remain on the electrode after 100 cycles. While for CuO@PPy anodes, the electrode structures maintain intact and the surface becomes more smooth. Undoubtedly, the protection of uniform PPy coating prevents CuO arrays falling off the substrate, suggesting good stability of the battery. Figure 3g-i shows cross-sectional images of the samples at different states. It is notable that the large volume expansion of CuO anode has occurred during the first discharge process and the following cycles' no significant volume changing can be observed. As illustrated in Fig. 1, CuO was gradually transformed to Cu_2O and Li_2O during the first discharge process, and the solid electrolyte interface (SEI) films were formed simultaneously, in which there is about 140% volume expansion. However, SEI films became stable and phase change occurred between Cu_2O and Cu, and the volume is no longer to change [49]. Based on this result, it can be inferred that PPy coatings can not only stabilize SEI films but also maintain electrode structure intact in the following cycles.

To well understand the functions of the PPy coatings, the electrochemical performances as anode materials for LIBs were evaluated. The cyclic performances and coulombic efficiencies (Fig. 4c, d) indicate that the specific capacity as well as the stability have been improved greatly for CuO@PPy anodes. The better coincidence of the impedance curves of CuO@PPy after cycling also indicates that the addition of PPy can promote the formation of SEI effectively. It can be seen from Table 1 that arrayed structures make the stability of pure CuO improved in certain degree, but the specific capacity is not enhanced significantly, and the PPy coatings make the discharge specific capacities enhanced more than 20%, and it has reached to 35.1% at 0.2 C for the 100th cycle. The stability of CuO@PPy is as good as expected when the battery is performed at low-current charge/discharge cycles, the capacity is not loss at 0.2 C from the 1st to the 100th cycles, while it is only 3.4% and 6.9% for 1 C and 2 C, respectively. As to pure CuO anodes, the reason can be explained by the different mechanisms of electrochemical process shown as Fig. 4e, f. On the basis of reported results, the electrochemical process

Table 2 Performance comparison with previously published literature

Samples	Capacity (mAh/g)	Current (mA/g)	Cycle number	Ref.
Tube-like carbon CuO	545.1	100	500	12
CuO nanostructures	590	670	100	13
Porous CuO hollow octahedra	470	100	100	14
CuO nanowires	461.5	100	100	20
Binder-free CuO nanosheet	540	100	50	26
Binder-free Cu(OH)2@CuO	521	67	80	29
Octahedral CuO wrapped 3D graphene	405	100	50	30
Our work: binder-free CuO@PPy	561	670	100	

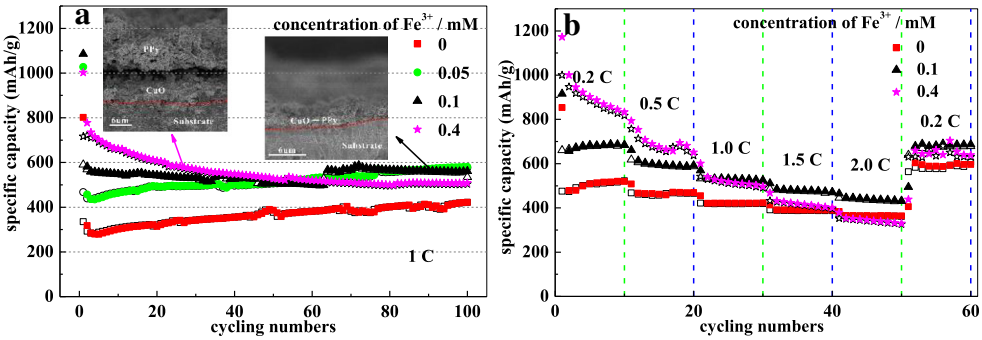

Fig. 5 The effect of PPy on the **a** stability and **b** c-rate performances of batteries

controlled by semi-infinite linear diffusion when the slope is near to 0.5 and dominated by surface capacitive-controlled process when *it near to* 1 [50]. At lower current densities, the electrochemical process controlled by semi-infinite linear diffusion and the capacity is mainly contributed to the embedding reactions of lithium in the bulk of CuO, in which the effect of phase transition is more significant. It is known that the phase transition may cause a large volume changing, which not only lead to the shedding of active materials but also the repeated forming of SEI films [51]. On the contrary, at higher current densities, the process is dominated by surface capacitive-controlled process, and the bulk diffusion of lithium ions is no longer the main reactions. The redox reactions on/near the surface of active materials are the main process, which is the pseudocapacitive charge storage [52]. In CV curves of CuO and CuO@PPy samples, the reduction peaks appearing at 0.67 V, 1.22 V can be assigned to the $Cu_2O + Cu_xO_y \rightarrow Cu + Li_2O$ electrochemical reactions. At the same time, the oxidation peak appearing at 2.52 V is the transition of $Cu \rightarrow Cu_2O$. It can be seen from Table 2 that the binder-free PPy@CuO anode shows better performance by comparison with other people's work [26, 29, 30] and better performance than some other anodes prepared by coatings [12, 14, 20].

Further investigation indicates that the amount of PPy coatings has a great influence on the electrochemical performance of CuO. Here, the coating amount of PPy is determined by the concentration of Fe^{3+}, and the higher the concentration of Fe^{3+}, the larger the coating amount of PPy. As shown in Fig. 5a, three type of CuO@PPy samples harvest higher specific capacities than the pure CuO sample from the initial cycle to the final cycle. Carefully analyzing, we find more than half of the enhanced capacity (about 150 mAh g^{-1}) is contributed to the lithium storage of PPy, which have about 80–90 mAh g^{-1} of theoretical specific capacity [39, 53, 54]. The result of the study does not mean the more the amount of PPy is, the more the capacity from PPy is increased. Clearly, when the concentration of Fe^{3+} is reached to 0.4 M, the stability and the capacities of the battery are also dropped greatly. The reason is that the high concentration of Fe^{3+} can accelerate polymerization of pyrrole, leading to ununiform coatings and surface accumulation of PPy on CuO (as shown in Fig. 5a insertion). As a result, 0.1 M Fe^{3+} is best for uniform coating PPy on the surface of CuO arrays, and the battery has higher capacity and better stability. Moreover, as shown in Fig. 5b (▲ marked), the capacity fading is only to 12%, 11%, 9.7%, and 8.1% when the current increases from 0.2 C to 0.5 C, 1 C, 1.5 C, and 2 C. CuO@PPy with proper coating (such as 0.1 M) exhibits an excellent rate performance and a capacity retention of 94.7% when the current returned from 2 to 0.2 C.

Conclusions

An effective method was reported in this paper for preparing uniform PPy coatings of CuO arrays. The amount of the PPy coatings can be controlled by the concentration of Fe^{3+} easily and the stability and the capacity of CuO anodes can be improved greatly with the help of the uniform PPy coatings. Moreover, it is found that the large volume expansion of CuO anode has occured during the first discharge process, and the following cycles no volume changing can be observed. It can be inferred that PPy coatings can not only stabilize SEI films but also maintain electrode structure intact in following cycles.

Funding information This work is financially supported by the Natural Science Foundation of Henan Province (Grant no. 162300410093) and the Key Science Foundation of Higher Education of Henan Province (Grant no. 19A140008).

References

1. Jiang Y, Jiang Z, Jiang ZJ, Liu M (2018) Phase and morphology evolution induced lithium storage capacity enhancement of porous CoO nanowires intertwined with reduced graphene oxide nanosheets. ChemElectroChem 5(23):3679–3687
2. Gou Q, Li C, Zhong W, Zhang X, Dong Q, Lei C (2019) Hierarchical structured porous N-doped carbon coating MnO microspheres with enhanced electrochemical performances as anode materials for lithium-ion batteries. Electrochim Acta 296:730–737
3. Li F, Luo G, Yu J, Huang W, Xu D, Chen W, Huang X, Yang S, Fang Y, Yu X (2019) Terminal hollowed Fe_2O_3@SnO_2

heterojunction nanorods anode materials with enhanced performance for lithium-ion battery. J Alloy Compd 773:778–787
4. Park GD, Hong JH, Park SK, Kang YC (2019) Strategy for synthesizing mesoporous NiO Polyhedra with empty nanovoids via oxidation of NiSe polyhedra by nanoscale Kirkendall diffusion and their superior lithium-ion storage performance. Appl Surf Sci 464: 597–605
5. Hou Q, Man Q, Liu P, Jin R, Cui Y, Li G, Gao S (2019) Encapsulation of Fe_2O_3/NiO and Fe_2O_3/Co_3O_4 nanosheets into conductive polypyrrole for superior lithium ion storage. Electrochim Acta 296:438–449
6. Cheng YW, Chen CH, Yang SW, Li YC, Peng BL, Chang CC, Wang RC, Liu CP (2018) Freestanding three-dimensional CuO/NiO Core–Shell nanowire arrays as high-performance lithium-ion battery anode. Sci Rep-Uk 8(1):18034
7. Tan G, Wu F, Yuan Y, Chen R, Zhao T, Yao Y, Qian J, Liu J, Ye Y, Yassar R, Lu J, Amine K (2016) Freestanding three-dimensional core–shell nanoarrays for lithium-ion battery anodes. Nat Commun 7(1):11774
8. Gusain R, Kumar P, Sharma OP, Jain SL, Khatri OP (2016) Reduced graphene oxide-CuO nanocomposites for photocatalytic conversion of CO_2 into methanol under visible light irradiation. Appl Catal B-Environ 181:352–362
9. Chen X, Chu D, Wang L (2019) One-step and green synthesis of novel hierarchical hydrangea flower-like CuO nanostructures with enhanced photocatalytic activity. Phys E 106:194–199
10. Zhang X, Zhou J, Dou W, Wang J, Mu X, Zhang Y, Abas A, Su Q, Lan W, Xie E, Zhang C (2018) Room-temperature vertically-aligned copper oxide nanoblades synthesized by electrochemical restructuring of copper hydroxide nanorods: an electrode for high energy density hybrid device. J Power Sources 383:124–132
11. Peng HJ, Hao GX, Chu ZH, He CL, Lin XM, Cai YP (2017) Mesoporous spindle-like hollow CuO/C fabricated from a cu-based metal-organic framework as anodes for high-performance lithium storage. J Alloy Compd 727:1020–1026
12. Chen Z, Hou Z, Xu W, Chen Y, Li Z, Chen L, Wang W (2019) Ultrafine CuO nanoparticles decorated activated tube-like carbon as advanced anode for lithium-ion batteries. Electrochim Acta 296: 206–213
13. Wang Z, Su F, Madhavi S, Lou XW (2011) CuO nanostructures supported on cu substrate as integrated electrodes for highly reversible lithium storage. Nanoscale 3(4):1618–1623
14. Wu R, Qian X, Yu F, Liu H, Zhou K, Wei J, Huang Y (2013) MOF-templated formation of porous CuO hollow octahedra for lithium-ion battery anode materials. J Mater Chem A 1(37):11126–11129
15. Reddy MV, Rao GVS, Chowdari BVR (2013) Metal oxides and oxysalts as anode materials for Li ion batteries. Chem Rev 113(7): 5364–5457
16. Lee KT, Cho J (2011) Roles of nanosize in lithium reactive nanomaterials for lithium ion batteries. Nano Today 6(1):28–41
17. Wu HB, Chen JS, Hng HH, Lou XW (2012) Nanostructured metal oxide-based materials as advanced anodes for lithium-ion batteries. Nanoscale 4(8):2526–2542
18. Gao S, Yang S, Shu J, Zhang S, Li Z, Jiang K (2008) Green fabrication of hierarchical CuO hollow micro/nanostructures and enhanced performance as electrode materials for lithium-ion batteries. J Phys Chem C 112:19324–19328
19. Cheong JY, Kim C, Jung JW, Yoon KR, Kim ID (2018) Porous SnO_2-CuO nanotubes for highly reversible lithium storage. J Power Sources 373:11–19
20. Wang Z, Zhang Y, Xiong H, Qin C, Zhao W, Liu X (2018) Yucca fern shaped CuO nanowires on cu foam for remitting capacity fading of Li-ion battery anodes. Sci Rep-Uk 8(1):6530
21. Wang G, Huang J, Chen S, Gao Y, Cao D (2011) Preparation and supercapacitance of CuO nanosheet arrays grown on nickel foam. J Power Sources 196(13):5756–5760
22. Li Y, Chang S, Liu X, Huang J, Yin J, Wang G, Cao D (2012) Nanostructured CuO directly grown on copper foam and their supercapacitance performance. Electrochim Acta 85:393–398
23. Wang C, Wang H, Matios E, Hu X, Li W (2018) A chemically engineered porous copper matrix with cylindrical Core–Shell skeleton as a stable host for metallic sodium anodes. Adv Funct Mater 28(30):1802282
24. Li Z, Li G, Xu W, Zhou M, Xu C, Shi M, Li F, Chen L, He B (2018) A facile and low-cost strategy to fabricate self-integrated porous leaf-like CuO nanoplate array-based anode for high-performance lithium-ion batteries. ChemElectroChem 5(19):2774–2780
25. Chen X, Zhang N, Sun K (2012) Facile fabrication of CuO mesoporous nanosheet cluster array electrodes with super lithium-storage properties. J Mater Chem 22(27):13637–13642
26. Yuan W, Qiu Z, Chen Y, Zhao B, Liu M, Tang Y (2018) A binder-free composite anode composed of CuO nanosheets and multi-wall carbon nanotubes for high-performance lithium-ion batteries. Electrochim Acta 267:150–160
27. Tang C, Zhang H, Jiao D, Hu R, Liu Z (2019) Hierarchical C-doped CuO nanorods on carbon cloth as flexible binder-free anode for lithium storage. Mater Design 162:52–59
28. Zhang Q, Zhou K, Lei J, Hu W (2019) Nitrogen dual-doped porous carbon fiber: a binder-free and high-performance flexible anode for lithium ion batteries. Appl Surf Sci 467:992–999
29. Chen W, Zhang H, Ma Z, Li S, Li Z (2018) Binder free cu$(OH)_2$/CuO electrodes fabricated directly on copper foils by facile large-scale production method. J Alloy Compd 762:565–573
30. Ji D, Zhou H, Tong Y, Wang J, Zhu M, Chen T, Yuan A (2017) Facile fabrication of MOF-derived octahedral CuO wrapped 3D graphene network as binder-free anode for high performance lithium-ion batteries. Chem Eng J 313:1623–1632
31. Lee S, Song H, Hwang JY, Kim SM, Jeong Y (2018) A novel free-standing anode of CuO nanorods in carbon nanotube webs for flexible lithium ion batteries. Carbon Lett 27:98–107
32. Liu Y, Ying Y, Mao Y, Gu L, Wang Y, Peng X (2013) CuO nanosheets/rGO hybrid lamellar films with enhanced capacitance. Nanoscale 5(19):9134–9140
33. Zoolfakar AS, Rani RA, Morfa AJ, Mullaned AP, Kalantar-zadeh K (2014) Nanostructured copper oxide semiconductors: a perspective on materials synthesis methods and applications. J Mater Chem C 2(27):5247–5270
34. Zoolfakar AS, Ahmad MZ, Rani RA, Ou JZ, Balendhran S, Zhuiykov S, Latham K, Wlodarski W, Kalantar-zadeh K (2013) Nanostructured copper oxides as ethanol vapour sensors. Sensor Actuat B-Chem 185:620–627
35. Li J, Li X, Wang H, Zhao Y, Sun Y, Sun X, Zhen Z, Li Q, Yang F (2018) Structural optical and electrical properties of polycrystalline CuO thin films prepared by magnetron sputtering. J Electron Mater 47(10):5788–5792
36. Wei S, Chen Y, Ma Y, Shao Z (2010) Fabrication of CuO/ZnO composite films with cathodic co-electrodeposition and their photocatalytic performance. J Mol Catal A-Chem 331(1-2):112–116
37. Wang C, Sawicki M, Emani S, Caihong L, Shaw LL (2015) $Na_3MnCO_3PO_4$–a high capacity multi-electron transfer redox cathode material for sodium ion batteries. Electrochim Acta 161:322–328
38. Wang C, Sawicki M, Kaduk JA, Shaw LL (2015) Roles of processing, structural defects and ionic conductivity in the electrochemical performance of $Na_3MnCO_3PO_4$ cathode material. J Electrochem Soc 162(8):A1601–A1609
39. Yuan T, Ruan J, Zhang W, Tan Z, Yang J, Ma ZF, Zheng S (2016) Flexible overoxidized polypyrrole films with orderly structure as high-performance anodes for Li-ion and Na-ion batteries. Acs Appl Mater Inter 8(51):35114–35122
40. Sun X, Zhang H, Zhou L, Huang X, Yu C (2016) Polypyrrole-coated zinc ferrite hollow spheres with improved cycling stability for lithium-ion batteries. Small 12(27):3732–3737

41. Wu L, Zheng J, Wang L, Xiong X, Shao Y, Wang G, Wang JH, Zhong S, Wu M (2019) PPy-encapsulated SnS_2 nanosheets stabilized by defects on TiO_2 support as durable anode material for lithium ion battery. Angew Chem Int Edit 58(3):811–815
42. Yin Z, Fan W, Ding Y, Li J, Guan L, Zheng Q (2015) Shell structure control of PPy-modified CuO composite nanoleaves for lithium batteries with improved cyclic performance. ACS Sustain Chem Eng 3(3):507–517
43. Beebee C, Watkins EB, Sapstead RM, Ferreira VC, Ryder KS, Smith EL, Hillman AR (2019) Effect of electrochemical control function on the internal structure and composition of electrodeposited polypyrrole films: a neutron reflectometry study. Electrochim Acta 295:978–988
44. Ma F, Zhang D, Zhang N, Zhang T, Wang Y (2018) Polydopamine-assisted deposition of polypyrrole on electrospun poly (vinylidene fluoride) nanofibers for bidirectional removal of cation and anion dyes. Chem Eng J 354:432–444
45. Wang H, Leaukosol N, He Z, Fei G, Si C, Ni Y (2013) Microstructure distribution and properties of conductive polypyrrole/cellulose fiber composites. Cellulose 20(4):1587–1601
46. Cho G, Fung BM, Glatzhofer DT, Lee JS, Shul YG (2001) Preparation and characterization of polypyrrole-coated nanosized novel ceramics. Langmuir 17(2):456–461
47. Zhang J, Wang S, Xu M, Wang Y, Xia H, Zhang S, Guo X, Wu S (2009) Polypyrrole-coated SnO2 hollow spheres and their application for ammonia sensor. J Phys Chem C 113:1662–1665
48. Tong L, Gao M, Jiang C, Cai K (2019) Ultra-high performance and flexible polypyrrole coated CNT paper electrode for all-solid-state supercapacitors. J Mater Chem A 7(17):10751–10760. https://doi.org/10.1039/c9ta01856e
49. Feng L, Wang R, Zhang Y, Ji S, Chuan Y, Zhang W, Liu B, Yuan C, Du C (2019) In situ XRD observation of CuO anode phase conversion in lithium-ion batteries. J Mater Sci 54(2):1520–1528
50. Luo P, Cui Z, Jia Z, Sun J, Tan Y, Guo X (2017) Monodispersed carbon-coated cubic NiP_2 nanoparticles anchored on carbon nanotubes as ultra-long-life anodes for reversible lithium storage. ACS Nano 11:3705–3715
51. Chen C, Wen Y, Hu X, Ji X, Yan M, Mai L, Hu P, Shan B, Huang Y (2017) Na^+ intercalation pseudocapacitance in graphene-coupled titanium oxide enabling ultra-fast sodium storage and long-term cycling. Nat Commun 6:6929
52. Li JM, Kurra N, Seredych M, Meng X, Wang HZ, Gogotsi Y (2019) Bipolar carbide-carbon high voltage aqueous lithium-ion capacitors. Nano Energy 56:151–159
53. Song Z, Qian Y, Gordin ML, Tang D, Xu T, Otani M, Zhan H, Zhou H, Wang D (2015) Polyanthraquinone as a reliable organic electrode for stable and fast lithium storage. Angew Chem Int Ed 54(47):13947–13951
54. Novák P, Müller K, Santhanam KSV, Haas O (1997) Electrochemically active polymers for rechargeable batteries. Chem Rev 97(1):207–281